UC Berkeley
UC Berkeley Previously Published Works

Title

Seismic displacement of gently-sloping coastal and marine sediment under multidirectional earthquake loading
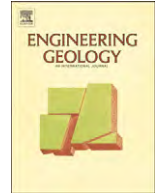
Permalink

Author

Kayen, Robert

Publication Date

DOI

CrossMark

Seismic displacement of gently-sloping coastal and marine sediment under multidirectional earthquake loading

Robert Kayen *

United States Geological Survey, Menlo Park, CA 94025, United States
University of California, Los Angeles, CA 90095, United States

A B S T R A C T

Gentle sediment-laden slopes are typical of the onshore coastal zone and offshore continental shelf and slope. Coastal sediment are commonly young weakly consolidated materials that are well stratified, have low strength, and can mobilize shear displacements at low levels of stress. Seismically-driven plastic displacements of these sediment pose a hazard to coastal cities, buried onshore utilities, and offshore infrastructure like harbor protection and outfalls. One-dimensional rigid downslope-directed Newmark sliding block analyses have been used to predict earthquake deformations generally on steeper slopes that are modeled as frictional materials. This study probes the effect of multidirectional earthquake motions on inertial displacements of gently sloping ground of the coastal and offshore condition where soft-compliant soil is expected. Toward that objective, this investigation seeks to understand the effect on Newmark-type displacements of [1] multidirectional earthquake shaking and [2] soil compliance. In order to model multidirectional effects, the earthquake motions are rotated into the local slope strike- and dip-components. On gently sloping ground, including the strike component of motion always results in a larger and more accurate shear stress vector. Strike motions are found to contribute to downslope deformations on any declivity. Compliant response of the soil mass also influences the plastic displacements. The magnitude of seismic displacements can be estimated with a simplified model using only the estimated soil yield-acceleration (k_y) and the peak ground velocity (V_{max}) of the earthquake motions. Compliance effects can be effectively mapped using the concept of Plastic Displacement Response Spectra (PDRS).

Published by Elsevier B.V.

1. Introduction

Broad regions of the world's coastal zone are composed of gently sloping deposits of Holocene and Pleistocene sediment and sedimentary terrace deposits. Onshore, and on the continental shelf, the slopes are exceedingly flat ranging from level ground to at most a few degrees. Globally, the width of the continental shelf is 70 km from shoreline-to-shelf break whose depth averages 135 m. That is, these environments are nearly level. Seismic displacements on the continental shelf occur on nearly level surfaces. Worldwide, the continental slope averages 4°. A study of the entire known-catalog of Atlantic coast seafloor mass movements by Booth et al. (1993) found that 70% of the failures occurred on slopes of 6° or less. One-half of the known Atlantic seafloor mass movements involve displacement of relatively thin bodies of sediment, no more than tens of meters in thickness, that cover areas of five-square kilometers, or less. The dominant mechanism of failure of these mass movements is infrequent earthquakes (Booth et al., 1993; Lee et al. 1993). The abundance of thin seafloor mass movements in weakly consolidated sediment on low angle slopes is counter to the experience of geologists on land who might ascribe the term 'landslide' to a steeper feature. Nevertheless, these gentle slopes of sediment are the dominant environment for earthquake-driven mass movements in the offshore and coastal zone.

Onshore, permanent seismic displacements of the ground have resulted in considerable damage to underground pipeline networks buried in soft young deposits. Pipeline breaks in non-liquefied ground have damaged urban buried infrastructure, for example during the Northridge earthquake (Trifunac and Todorovska, 1997; O'Rourke, 1998) and the Hyogo-Nambu Earthquake (e.g. Loukidis et al., 2001).

Over one-hundred years ago, the American geologist Grove Karl Gilbert, reported on the geologic aspects of the 1906 M7.8 San Francisco, California earthquake (Lawson, 1908) and described nearly 10 m of seismic displacement in Tomales Bay sediment at Point Reyes, north of San Francisco. The noteworthy aspect of his observation was the upslope movement on a gentle slope.

'It is a notable feature of this displacement that the disturbed material moved up the slope instead of down, so that the transfer was not only independent of gravity but opposed to it. The phenomenon, therefore, does not fall in the same category with landslides, and if properly interpreted it may throw light on the mechanics of the earthquake pulses.'

[–G.K. Gilbert (Lawson, 1908)]

* Corresponding author at: University of California, United States.
  E-mail address: rkayen@ucla.edu.

Nomenclature

a_c	critical yield acceleration of Wilson and Keefer (1985)
A_c	correction of isotropically-consolidated shear test results to represent anisotropic field conditions
a_n	dimensionless stiffness and geometry parameter for a wedge embankment (Ambraseys, 1960).
A_r	measured of the degradation of strength due to repeated cyclic loading, determined through cyclic triaxial shear testing degradation during cyclic loading
a	acceleration from an earthquake time history
F_D	total dynamic load on the sliding plane
F_{eq}	Earthquake inertial force
F_α	slope gravitational force
F_c	damping force
F_k	stiffness force
g	acceleration due to gravity, 9.81 m/s
h_w	depth of the water table
H	total sliding mass thickness
I_h	two-component horizontal Arias intensity of either the relative motion of the sliding mass or the earthquake base motion
I_n	ratio of the relative Arias intensity of the 2-component sliding mass normalized by the 2-component Arias intensity of the earthquake base motion
k	partitioned mass shear-stiffness element
k_y	yield acceleration
k_{max}	peak ground acceleration
M_r	mass ratio, m_1/M_T
m_1	upper mass of partitioned block
m_0	lower mass of partitioned block
M_T	total mass of block
NSP	Normalized Strength Parameter approach of Ladd and Foott (1974), based on the assumption that strength parameters normalized by their consolidation stress are constant for a given sediment with a given OCR
OCR	overconsolidation ratio ($\sigma'_{vm}/\sigma'_{vo}$) measured through consolidation testing
p	the average normal effective stress acting on a mass
q	shear stress acting on a mass
S	effective stress normalized-normally consolidated shear strength adjusted for dynamic loading and anisotropy factors
S_u	undrained shear strength
S_n	ratio of the static undrained shear strength of a normally consolidated sediment to its consolidation stress
Δt	earthquake recording time step increment
T	fundamental mode period of slope or truncated wedge
u_{max}	Maximum sliding displacement
$\ddot{u}_b$	Acceleration beneath the failure plane
$\ddot{u}_o$	Relative acceleration of the lower mass above the failure plane
$\dot{u}_1$	Relative velocity of the upper mass
u_1	Relative displacement of the upper mass
V_{max}	peak ground velocity (PGV) of earthquake motion
V_s	Shear wave velocity
α	slope angle (degrees)
γ	bulk density of a sediment
γ_w	density of fresh water (1.00 g/cm^3), or seawater (1.025 g/cm^3)
Λ_0	overconsolidation power function
η	log of the ratio of k_y and V_{max},
ϕ	Mohr-Coulomb angle of effective shear resistance
σ_{vo}	in-place vertical total stress exerted by the weight of overburden material
σ'_{vo}	in-place vertical effective stress exerted by the weight of overburden material
σ'_{vm}	maximum past vertical effective stress exerted on a soil material.
τ_d	driving stress vector
τ_y	yield stress
τ_{dip}	total shear stress in the dip direction
τ_{strike}	total shear stress in the strike direction
$\tau_{eq,d}$	earthquake inertial stress in the dip direction
$\tau_{c,d}$,	mobilized viscous damping stress in the dip direction
$\tau_{k,d}$	mobilized stiffness stress in the dip direction
$\tau_{eq,s}$	strike motion inertial stress
$\tau_{c,s}$	strike-mobilized viscous damping stress
$\tau_{k,s}$	strike-mobilized stiffness stress
θ	azimuth of the total stress vector

Gilbert recognized that the displacement in soil was driven upslope by earthquake motion, counter to the gravitational direction of normal slope mass movements. The observation that earthquake motions could drive displacements upslope in a gently sloping environment was an important contribution, though in Gilbert's time no practical method was available to evaluate the interaction of gentle soil slopes and earthquake motions.

Nathan Newmark (1965) presented a computational method for assessing the seismic displacement potential of slopes. The method assumes rigid-plastic behavior of sloping ground subjected to loading by an acceleration time history. Block displacement begins when the yield acceleration, k_y, of the sliding mass is exceeded by the earthquake acceleration.

This paper explores the effects of multidirectional ground motion and soil compliance in order to understand how soil slides develop on gentle slopes typical of the coastal plain and offshore shelf and slope. Including multidirectional seismic shaking leads to the computation of complex trajectories of plastic seismic-displacements. A fundamental aspect of the approach is the analysis of the local-slope strike and dip motions, that are rotated from the two orthogonal ground motions typically recorded in the east-west and north-south directions. The strike and dip motions are used compute shear stress on the soil mass in both the strike and dip directions. Plastic deformation occurs when the combined loads exceed the capacity of the soil mass to resist yielding.

The original Newmark (1965) formulation analyzed downslope dip-directed motion and assumes a rigid-plastic behavior of the sliding ground. Typically, when applying Newmark analyses, practitioners use the component of motion that contains the peak ground acceleration and neglect the effect of the orthogonal component of motion. A modern implementation of the rigid 1-D Newmark approach with a strain softening element can be found in Jibson et al. (2013). Work by Goodman and Seed (1966), Seed and Martin (1966), Ambraseys and Sarma (1967) and Makdisi and Seed (1978) extended Newmark's original method, incorporated soil compliance, and provided practitioners with simplified procedures for estimating seismic displacements of slopes. Two alternate approaches have been used to address the dynamic response of soft ground. A decoupled procedure developed by Seed et al. (1973), and Seed (1979), involved computation of the elastic response of a compliant soil mass along a potential failure plane, assuming no displacement. The computed averaged motion at the depth of the potential failure plane, termed the Horizontal Equivalent Acceleration, is used to compute permanent displacements in a separate rigid-plastic Newmark analysis. This approach decouples the compliant response of

the sliding mass from the displacement on the sliding plane. Work by Bray and colleagues has extended the decoupled approach to the dynamic response of landfills (Augello et al., 1995; Bray et al., 1993; Bray et al., 1995; Bray and Repetto, 1994; Rathje and Bray, 2000).

Coupled-methods include the compliant response in the calculation of displacements (Lin and Whitman, 1983; Kramer and Smith, 1997; Rathje and Bray, 2000; Gazetas and Uddin, 1994). Compliant models include a damped lumped-mass structure that allows for the upper mass to shake in response to motions produced by earthquake shaking beneath the sliding plane. Kramer and Smith (1997) found that the displacements were sensitive to the interaction of the earthquake motion and the natural period of the compliant-block above the slide plane. Kramer and Smith (1997) used a concept termed 'slope spectra' to describe the relative-amplification of displacements in a compliant model. Application of the coupled and decoupled methods indicate that the decoupled approach generally produces good, somewhat conservative, displacement predictions. Both coupled and decoupled compliant models compute seismic displacements that can vary significantly from those predicted using the rigid-plastic Newmark approach.

Although these advancements have improved the applicability of the Newmark approach, several critical limitations restrict its application in the evaluation of seismic displacements: Firstly, the mass is assumed to conform to an infinite slope formulation that might not be a realistic representation of the affected mass. Secondly, uniform soil properties are assumed to act on the shear plane, and in the case of compliance throughout the soil mass. These properties are variable within and beneath the displaced block, and incorporating the probabilistic distribution of the soil properties is not currently done. Thirdly, the mass is assumed to move as a uniform material, though ground that is displaced tends to break into multiple coherent blocks that interact. Finally, the strain dependent nonlinearity of geotechnical properties is not easily modeled in Newmark analysis and typically neglected.

2. Dynamic displacements in compliant sediment

A simple and direct approach for incorporating a coupled compliant system into the Newmark displacement model is to describe the potential slides as a viscously damped lumped mass. This paper presents a compliant model formulation similar to Kramer and Smith (1997), modified to include multidirectional motions. Modification of the Newmark one-dimensional (1-D) rigid-plastic block into a lumped-mass system involves partitioning the soil block above the slide plane into a lower mass, m_0, and an upper mass, m_1 (Eq. (1)). The mass partitioning ratio, M_r, is the ratio of the upper mass, m_1, and the total mass, M_T.

$$M_r = \frac{m_1}{m_0 + m_1} = {}^{m_1}/_{M_T}. \tag{1}$$

A complete list of terms used in the equations is presented in the nomenclature list at the end of the paper. The compliant damping element, c, and shear stiffness element, k, are built into the partitioned mass-system and acted on by the upper mass velocity, $\dot{u}_1$, and displacement, u_1, respectively. With their inclusion, the induced load on the sliding plane, F_D, is the sum of the inertial force, F_{eq}; slope gravitational forces, F_α; damping force, F_c; and stiffness force, F_k (Kramer and Smith, 1997). The inertial force is a product of the lower mass ratio portion $(1 - M_r)$ of the total soil mass and the slope parallel component of the horizontal base-motion $(\ddot{u}_b)$. The static gravitational force, F_α acting on the slope is a function of the effective stress of M_T (σ_{vo}'). The viscous damping force, F_C, and shear stiffness force, F_K, are the mobilized through of the relative-velocity and -displacement, between the m_1

and m_0.

$$F_D = F_{eq} + F_\alpha + F_c + F_k = -(1-M_r)\frac{\sigma_{vo}}{g}cos\alpha\cdot\ddot{u}_b + \frac{\sigma_{vo}'}{g}cos\alpha\ sin\alpha + c\dot{u}_1 + ku_1. \tag{2}$$

The forces in Eq. (2) are appropriate for dip-directed downslope motions. For the strike slope-parallel direction, F_α is zero.

Loads on the base of the compliant slide mass require computation of motions within the mass to determine the elastic and viscous forces. The equation of motion of the upper mass is presented in Eq. (3), noting the addition of the upper mass acceleration, $\ddot{u}_1$, velocity, $\dot{u}_1$, and displacement, u_1, and the addition of the m_0 block acceleration, $\ddot{u}_0$, relative to the acceleration beneath the failure plane, $\ddot{u}_b$ (Kramer and Smith, 1997):

$$m_1\ddot{u}_1 + c\dot{u}_1 + ku_1 = -m_o(\ddot{u}_b + \ddot{u}_0). \tag{3}$$

The computed motions in the upper and lower masses make use of the Newmark beta-method of finite differences (Newmark, 1959; Chopra, 2001). Field measurement of stiffness of a soil mass is made through measurement of the shear wave velocity, V_s. Material damping ratio characteristics are typically determined through controlled laboratory testing (Zhang et al., 2005) or estimated from the literature.

3. Multidirectional trajectory of displacements

Multidirectional displacement analysis requires that we compute the resultant stress vector for all the strike and dip loads (inertial-stress, slope gravitational-shear stress, viscous damping-shear stress, and stiffness-shear stress. In the strike direction, the slope gravitational shear stress is equal to zero.

A comparison of the resultant vectors computed by the original 1-D Newmark rigid-plastic model and the compliant multidirectional model is shown in Fig. 1, here presented as stresses on a critical state yield surface. The plot looks down the hydrostatic confining stress axis of a conical yield surface drawn in shear stress-normal confining stress (q − p′) space, with the strike directions horizontal and dip directions vertical (Fig. 1a). It can be seen that the rigid model (Fig. 1b) utilizes only the downslope gravitational stress and stresses associated with the dip-directed earthquake motion to determine when yielding occurs. The multidirectional compliant model utilizes stresses in the strike and dip direction for inertial loads, the downslope gravitational stress, and the multidirectional compliant loads. As such, the multidirectional compliant model can yield in any direction on the slide plane in response to the multidirectional earthquake motions. The magnitude of the driving multidirectional stress vector, τ_D, is computed in Eq. (4).

The traditional 1-D dip-slope Newmark model undergoes yielding if the sum of the combined gravitational and inertial dip-slope vectors project outside the soil yield stress surface (τ_y). The direction of yielding in a 1-D model can only occur downslope or upslope. On the other hand, the resultant multidirectional stress vector, τ_D, can drive yielding along any azimuth.

$$\tau_D = \left(\sum\tau_{dip}{}^2 + \sum\tau_{strike}{}^2\right)^{1/2}. \tag{4}$$

Expanding the computed bidirectional resultant stress vector into the strike (τ_{strike}) and dip components (τ_{dip}) of stress (Eq. (5)), the total 'dip'-component is composed of slope stress, τ_α, inertial stress, $\tau_{eq,d}$, mobilized viscous damping stress, $\tau_{c,d}$, and mobilized stiffness stress, $\tau_{k,d}$. The total 'strike'-component of stress is composed of the strike motion inertial stress, $\tau_{eq,s}$, strike-mobilized viscous damping
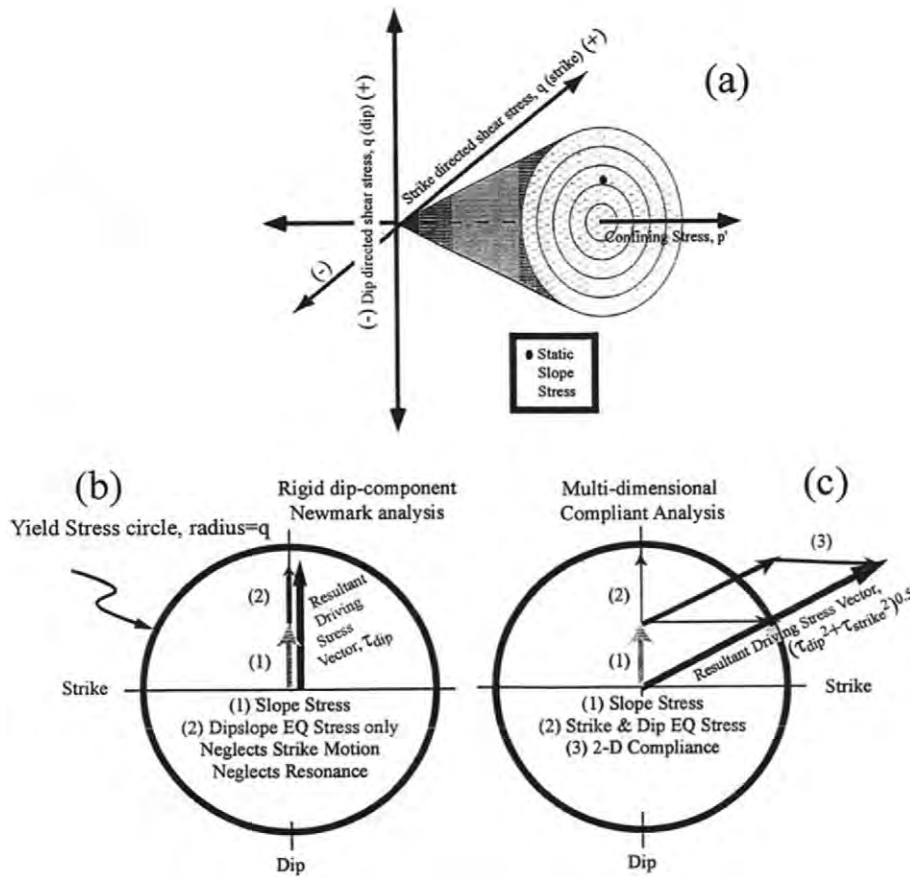
Fig. 1. (a) Oblique view of yield surface drawn in q-p′ space, (b) looking down the hydrostatic line, the total resultant stress-vector and yield surface for 1-D rigid Newmark analysis, and (c) total resultant stress vector for the multidirectional compliant model. The two yield surfaces have the same slope-induced static stress and dip directed earthquake stresses. The resultant vectors are different due to the additional strike motion and compliant stress. For the 1-D rigid Newmark condition (b) the slope gravitational shear stress [1] and dip-motion directed earthquake stress [2] are added to compute a total stress vector. For the 2-D compliant model (c) the total stress vector is the sum of the slope gravitational shear stress [1], the oblique earthquake motion resolved into strike and dip components [2] , and the oblique compliant stresses resolved into strike and dip components [3].

stress, $\tau_{c,s}$, and strike-mobilized stiffness stress, $\tau_{k,s}$.

$$\tau_D = \left(\sum \tau_{dip}^2 + \sum \tau_{strike}^2 \right)^{1/2}$$
$$= \left[\left(\tau_\alpha + \tau_{eq,d} + \tau_{c,d} + \tau_{k,d} \right)^2 + \left(\tau_{eq,s} + \tau_{c,s} + \tau_{k,s} \right)^2 \right]^{1/2}. \quad (5)$$

Multidirectionality has an important influence on inertial displacements of gently sloping ground. On all sloping ground the soil mass is confined anisotropically due to the initial static gravitational downslope shear stress and, therefore, plots off the hydrostatic-line. The consequence of this anisotropy is that strike-directed stresses that exceed the yield surface will produce both strike and dip-directed shear displacements on sloping plane. Indeed, on sloping ground even polarized strike-directed motions will displace a soil mass downslope. It can also be seen in Fig. 1 that neglecting the strike motion when computing the total stress vector underestimates the total applied shear stress on the potential failure plane. Traditional 1-D downslope Newmark displacement models underestimate the driving loads. On gently sloping ground, the underestimation of the stress vector can lead to an underestimation of computed displacements.

When the applied stress vector exceeds the yielding stress of the soil, displacements occur whose magnitude and azimuth are controlled by the associated flow rule (Wood, 1991). From the net stress components, the incremental shear-inducing strike- and dip-accelerations, velocities, and displacements are computed.

The azimuth of the total stress vector, θ, is:

$$\theta = tan^{-1} \left[\frac{\sum \tau_{strike}}{\sum \tau_{dip}} \right]. \quad (6)$$

Along this azimuth, the net exceedance of the applied stress-vector relative to the yield surface is broken into corresponding strike- and dip-components.

4. Soil yielding

To formulate a generalized conceptual model for the yielding of soil, the angle of internal frictional (ϕ) is commonly used for 1-D Newmark analysis. In this study focused on gentle coastal margin environments, an alternative approach is presented to formulate a yield acceleration for soil based on the Normalized Soil Parameter (NSP) framework of (Ladd and Foott, 1974). The NSP model is widely used in geotechnical engineering to characterize the strength of soil and is used for sediment whose strength parameters, normalized by their consolidation stress, are constant for a sediment of given overconsolidation ratio, OCR, the ratio of maximum past effective stress a soil has experienced to the in situ effective overburden stress. For these materials, the undrained-strength, S_u, mobilized during shear can be expressed as the effective stress normalized-normally consolidated shear strength, S_n, the overconsolidation ratio (OCR) measured through consolidation testing,

and a power function, Λ_0 (Ladd and Foott, 1974), as presented in Eq. (7):

$$\frac{S_u}{\sigma\prime_{vo}} = S_n(OCR)^{\Lambda_0}. \tag{7}$$

Lee and Edwards (1986) extended the NSP approach for the analysis of dynamic loading using laboratory consolidation and triaxial shear strength data. They defined a new term, S, the effective stress normalized-normally consolidated shear strength adjusted for dynamic loading and anisotropy factors. The parameter A_r is a measure of the degradation of strength due to repeated cyclic loading, determined through cyclic triaxial shear testing. The parameter A_c corrects of isotropically-consolidated shear test results to represent anisotropic field conditions. Eq. (8) presents the normalized strength accounting for these factors,

$$S = \frac{S_u}{\sigma\prime_{vo}} = A_c A_r S_n(OCR)^{\Lambda_0}. \tag{8}$$

The yield acceleration, k_y, is the critical minimum acceleration at which shear failure can begin. The yield acceleration, k_y, associated with the undrained peak shear strength of a fine grained soil can be determined through laboratory triaxial shear and consolidation testing. The yield acceleration, also termed the critical acceleration a_c by Wilson and Keefer (1985) are the same, and relate (1) the applied shear stress, τ_D and (2) mobilized shear strength, S. Newmark (1965), and subsequently Wilson and Keefer (1985), developed a simplified model for a_c that is a function of the slope factor of safety, dependent on the frictional properties of the sliding plain, total normal stress, and slope angle. Here, an alternative simplified yield acceleration, k_y, is solved in effective stress terms, relating the applied slope shear stress and resisting NSP-based strength that is function of the water table depth, h_w, the densities of the water, γ_w, and soil, γ, total slide thickness, H, and the slope angle, α (Eq. (9)):

$$k_y = \left[1 - \frac{\gamma_w}{\gamma}\left(1 - \frac{h_w}{H}\right)\right] \cdot \frac{A_c A_r S_n(OCR)^{\Lambda_0} - sin\alpha}{cos^2\alpha}. \tag{9}$$

Displacement on a slide plane occurs when the ground acceleration exceeds the yield acceleration of the soil mass. Ground beneath the overlying block accelerates faster than the block can maintain without undergoing shear. Relative displacements continue until the acceleration of the ground below the block falls below the yield acceleration. Deceleration occurs until the relative velocity of the block returns to zero.

5. Displacement model results

In this study, 55 close-in (<30 km) strong-motion records from seven California earthquakes are used to compute inertial two-dimensional plastic displacement trajectories. Motions were selected to cover a wide range of moderate-to-high intensity peak-acceleration levels (typically 0.3 g–l.0 g) and peak-velocity levels (typically 0.2 m/s-to-1.0 m/s). The two horizontal components of earthquake motion are rotated using a Pythagorean transformation from their original orientation (typically, North-South or Transverse-Parallel) into the strike-and-dip orientation of the modeled slope. To maintain computational stability of the Newmark beta-method (Chopra, 2001), the earthquake motions were also reprocessed from a coarse-time step (typically $\Delta t = 0.02$ s) to a fine-time step (typically $\Delta t = 0.005$ s).

To compute a displacement trajectory for a given acceleration time history, the initial soil strength-parameters and slope inclinations are used to determine the yield acceleration. Each displacement trajectory is computed by varying the soil strength, the slope angle, the azimuth of the slope, and the ground motion. It is easier to drive a soil mass downslope with up-dip directed seismic accelerations, than the reverse. However, on low slope angles a strong base-acceleration pulse can induce plastic displacements in the block in the upslope direction, as well as oblique strike and dip directions. For example, in Fig. 2, a block gently inclined to the south and subjected to the two horizontal components of the Newhall record from the 1994 Northridge Earthquake is initially driven up-slope to the north in response to a single pronounced long-duration acceleration spike. The plastic displacement trajectories and plastic displacement time histories in Fig. 2 present the relative displacement motions of the sliding mass (Fig. 2, left column), and the corresponding dip (Fig. 2, center column) and strike (Fig. 2, right column) displacements.

The three rows of solutions in Fig. 2 are for a slide mass on level ground 0°; and sloping ground at 2° and 4°. Material properties for all these solutions are the same. In frame 0°a, the distinction between maximum plastic shear displacement and final resting plastic displacement can be seen. Often, on slopes <4°, the maximum displacement occurs before the end of the earthquake record and can greatly exceed the final displacement. For certain types of buried utilities or infrastructure the maximum displacement may be a more important parameter than final displacement. Post-earthquake observations, and empirical models based on them are measurements of the final resting plastic shear displacements and thus may underestimate the maximum displacement that led to observed damage. When the slope steepens to 4°, or greater (see frame 4°a), the maximum and final plastic displacements almost always coincide. Nevertheless, on steeper slopes multidirectionally-computed displacements always exceed one-dimensional Newmark displacements.

On level ground conditions, the soil mass initially slides northward; then eastward; and finally westward. Most of the plastic displacement is northward and occurs within a narrow 2-s window. The maximum shear displacement is 61.8-cm toward N008E, whereas the final plastic shear displacement is 42.0-cm toward N009W. When the slope steepens to 2° toward the south, the effect of the declivity is to drive the soil mass ultimately downslope, despite the initial fling pulse that sends the slide mass up-slope. The maximum shear displacement is 45.2-cm toward NO 12E, whereas the final resting site for the slide is in the opposite direction at 16.4-cm toward S016W. That is, the slide is initially driven up-slope to its maximum plastic displacement, but ultimately comes to a resting position downslope of the starting pre-slide position. When the ground slope is elevated to 4°, the static slope stress contributes significantly to the accumulating displacements. The maximum and final plastic shear displacements are, at last, coincident at 115.7-cm toward S001W. The coincidence of maximum and final deformations is typical of moderate-to-steeply sloping ground with slopes >5°.

Displacement trajectories, like those presented in Fig. 2, are computed in 24,000 model runs of the compliant-Newmark model using California ground motion records from earthquakes ranging from 6.5–7.3, and slope angles ranging from 0°–4°. The results of displacements from these model runs are put into the form of k_y/k_{max} and compared with the displacement bands presented by Makdisi and Seed (1978) in Fig. 3. The parameter k_{max} is the peak acceleration of the base motion. The mean computed displacements in this model compared well within the mean response of the M = 6.5 band of Makdisi and Seed, and on average below the M = 7.5 band (Fig. 3), though this model shows a wider range of maximum displacements for a given value of k_y/k_{max} than is presented in the M = 6.5 Makdisi and Seed bands. Makdisi and Seed (1978) used four strong motion records to compute the bands in Fig. 3. The author attributes the broadness of the maximum displacement bands presented (<10 cm) a multidirectional shaking model appears to compute larger displacements than those presented by Makdisi and Seed (1978).

If the increased broadness of the k_y/k_{max} bands is attributable to a larger suite of ground motions, it may indicate that the variance in predicted displacements is principally dependent on the characteristics of the earthquake motion rather than the characteristics of the yield acceleration. This observation is consistent with field observations and
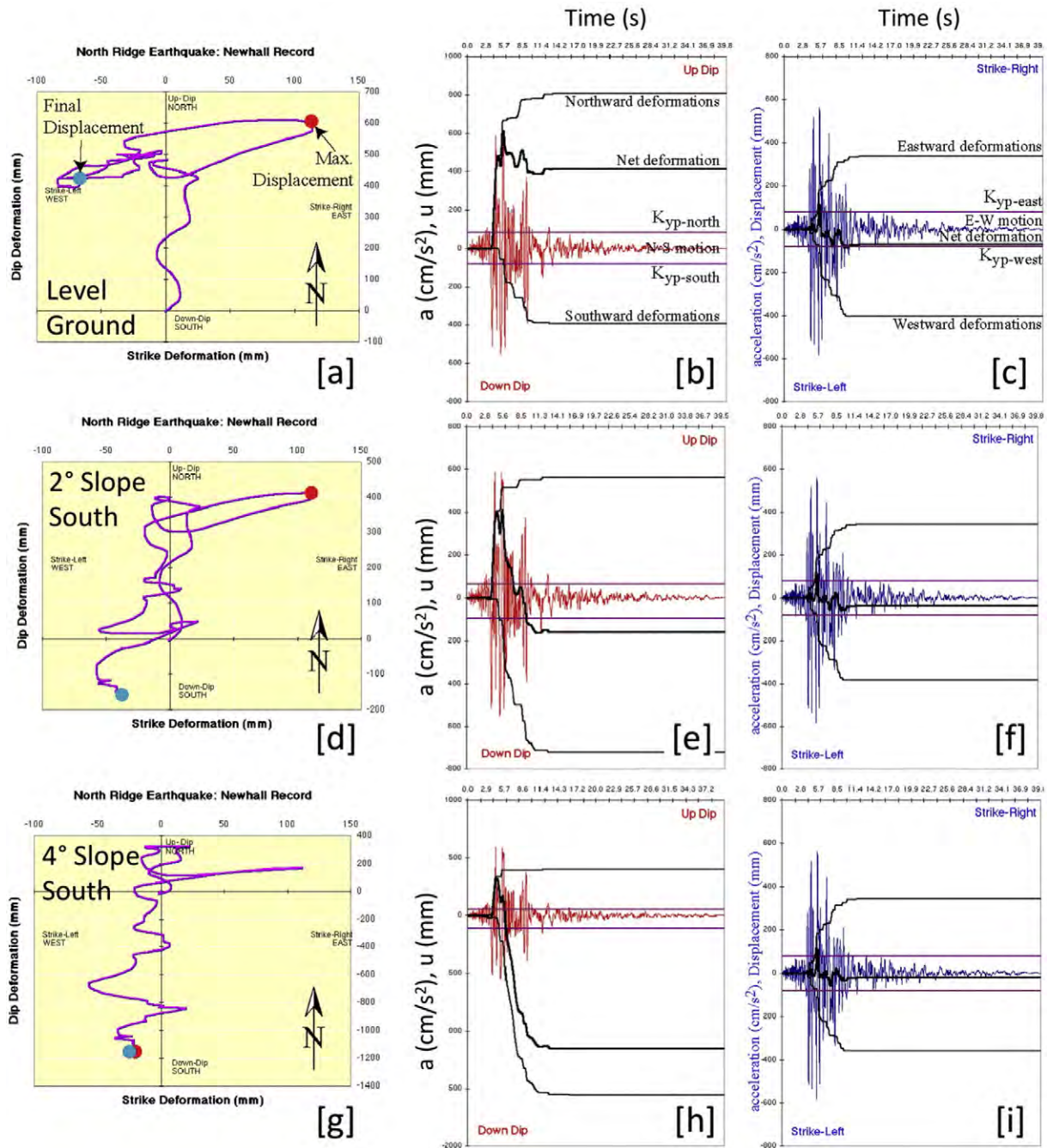
Fig. 2. Displacement trajectories for 0°, 2° and 4° sloping ground using the Newhall motion from the M6.7 Northridge 1994 earthquake. The left column shows a plan-view displacement trajectory (a), the center column shows the dip-directed motion and displacement (b), and the right column shows strike-directed motion and displacement (c).

modeling of Wilson and Keefer (1985) and Jibson (2007). Similar comparisons are possible with the more recent model of Bray and Travasarou, 2007, for their simplified procedure for estimating earthquake-induced slope displacements that includes the fundamental period of the slide mass.

A suite of alternate parameters were investigated to find a better predictor of maximum displacement than the traditional use of k_y/k_{max}. Arias intensity was no better at predicting displacements than k_y/k_{max}, although a useful measure that yields considerably better predictions of maximum displacement is a relationship based on k_y/V_{max}, where V_{max} is the peak ground motion velocity. A proxy for k_y/V_{Max} is the normalized Arias intensity parameter, I_n. The parameter I_n is the ratio of the 2-component plastic sliding accelerations of the slide mass normalized by the 2-component Arias intensity (I_h, Kayen and

Mitchell, 1997) of the earthquake base motion (Eq. (10)). Arias intensity (Arias, 1970) is proportional to the integral of the square of the acceleration values over time in a strong motion recording, or in the relative block sliding motion. For a block that undergoes no plastic displacement, there is no sliding motion and I_n equals zero. For a fully decoupled soil mass that accumulates plastic displacements in mirror opposite to the base acceleration pulse, I_n equals one. All plastic displacements (on level ground) fall between 0 and 1. Thus, I_n is a normalized measure of decoupling or detachment. On sloping ground, gravitationally-driven displacements can amplify the value of I_n.

$$I_n = \frac{I_h(\text{relative slide motion})}{I_h(\text{base motion})} = \left. \int_{t=0}^{\infty} a^2 dt \ (\text{slide motion}) \middle/ \int_{t=0}^{\infty} a^2 dt \ (\text{base motion}) \right. \quad (10)$$
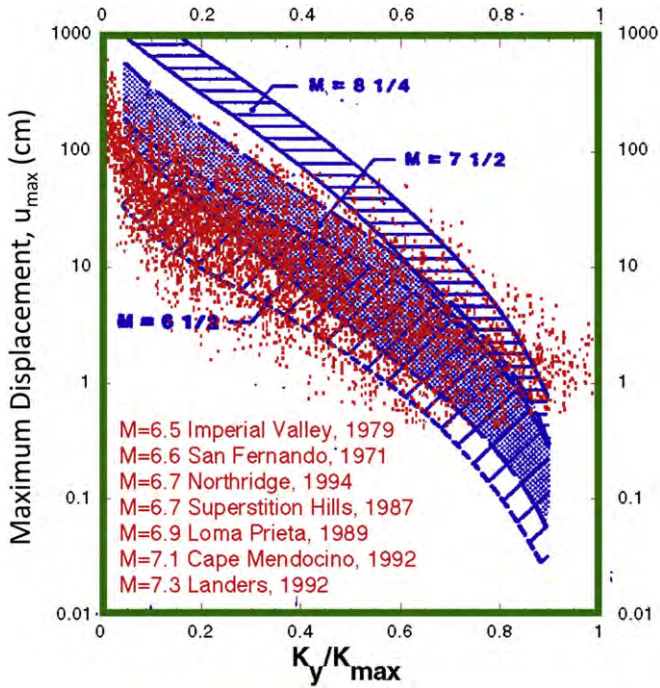
Fig. 3. Model solutions for 24,000 computed results plotted on the k_y/k_{max} bands of Makdisi and Seed (1978). At low levels of displacement (<10 cm) the multidirectional model computes larger displacements than that of Makdisi and Seed (1978) bands for M6.5 and M7.5.

The parameter I_n cannot be measured in the field without surface and downhole instrumentation, and could only be measured after sliding. However, this study found that I_n can be predicted knowing k_y/V_{max}, and that the seismic displacements are best predicted through a multi-parameter relationship of the parameters k_y and V_{max}. First, through modeling it was found that the product $I_n * V_{max}$ best predicted maximum shear displacements with less variance than the traditional k_y/k_{max} approach. The regression line in Fig. 4 presents the mean predicted maximum displacement of the slide mass. The standard deviation of maximum displacement is 70% of the mean for a given value of $I_n * V_{max}$, approximately one-quarter the standard deviation of the results based on k_y/k_{max}. The maximum permanent displacement can be
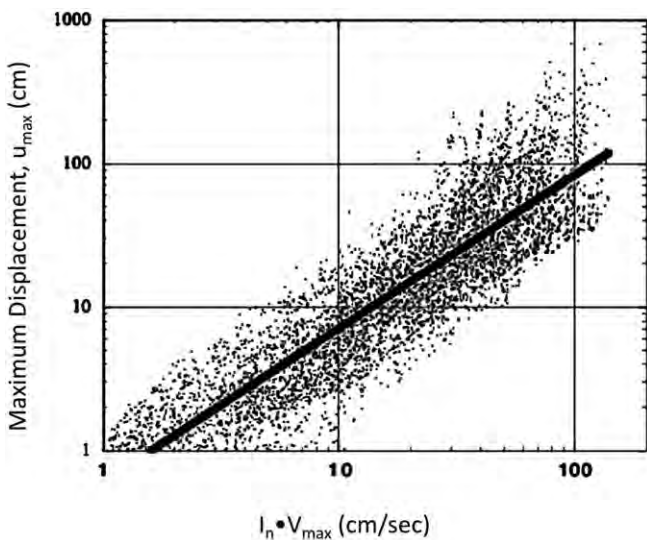

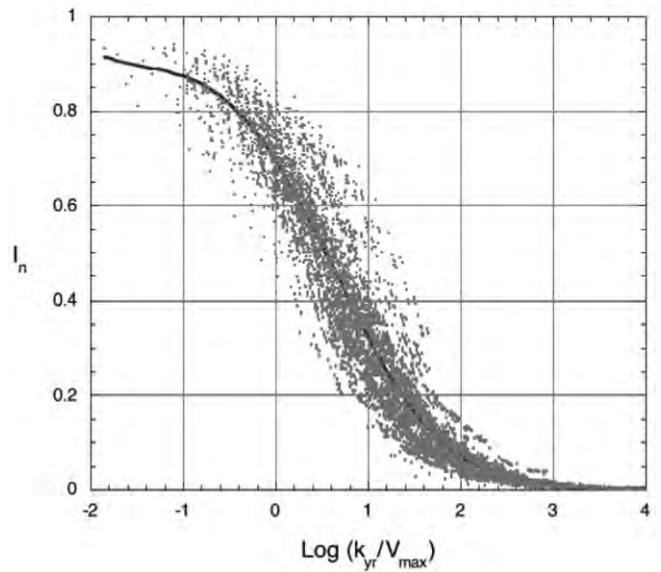**Fig. 4.** Model solutions for 24,000 computed results of maximum displacement versus $I_n \cdot V_{max}$.

Fig. 5. The parameter I_n versus $Log(K_y/V_{max})$.

predicted from the following Eq. (11):

$$u_{max}(cm) = 0.60856(I_n * V_{max})^{1.0691}, R = 0.64. \tag{11}$$

Although the parameter I_n cannot be measured prior to actual slide displacement, Fig. 5 presents modeled values of I_n versus k_y/V_{max}. The form of the polynomial regression describing I_n in terms of k_y/V_{max} is shown in Eq. (12), where the Thetas are parameter coefficients of the model variables:

$$I_n = \Theta_0 + \Theta_1 \cdot Log\frac{k_y}{V_{max}} + \Theta_2 \cdot Log\left(\frac{k_y}{V_{max}}\right)^2 + \Theta_3 \cdot Log\left(\frac{k_y}{V_{max}}\right)^3 + \ldots$$
$$+ \Theta_n \cdot Log\left(\frac{k_y}{V_{max}}\right)^n. \tag{12}$$

In the simplified regression the symbol eta, η, is substituted for the $Log(k_y/V_{max})$ in Eq. (13).

$$\eta = Log\frac{k_y}{V_{max}}. \tag{13}$$

The regression below in Eq. (14), presents I_n as a function of eta (η), and whose values range between −2 and 4. For η less than −2, the decoupling parameter I_n is approximately 1 (perfect sliding); for $\eta > 4$, I_n is 0 (no sliding). The correlation determination of the I_n regression is 0.963 and the standard deviation is 0.014 (3.15% of the average mean value of I_n). The combined standard deviation of Eqs. (11) and (14) is 71% of the mean value of the predicted maximum displacement.

$$I_n = 0.69387 - 0.30837\eta - 0.11782\eta^2 + 0.037173\eta^3 + 0.024655\eta^4 - 0.004181\eta^5$$
$$- 0.0023717\eta^6 + 0.00025628\eta^7 + 0.00013515\eta^8 - 0.000020304\eta^9. \tag{14}$$

Eq. (15) combines Eqs. (11) and (14). To compute displacements using Eq. (15), estimate the yield acceleration of the soil system with Eq. (9) given the soil properties and local slope geometry. An estimate of the peak ground velocity can be made using attenuation equations (e.g. Boore et al., 2014), or determined directly from strong motion

time history records.

$$u_{max}(cm) = 0.60856(V_{max}(0.69387-0.30837\eta-0.11782\eta^2+0.037173\eta^3 \quad (15)$$
$$+0.024655\eta^4-0.004181\eta^5-0.0023717\eta^6+0.00025628\,\eta^7$$
$$+0.00013515\eta^8-0.000020304\eta^9))^{1.0691},$$
$$R = 0.64.$$

6. Plastic Displacement Response Spectra

Soils are compliant and resonate when excited by input motions. Resonance effects are important in displacement computation of thick and soft soil deposits, low-shear wave velocity landfills and tall engineered-soil embankments. The interaction of earthquake motion and soil compliance can amplify or de-amplify the predicted permanent displacements relative to traditional rigid Newmark displacement predictions. Normalizing the displacements computed by a 2-D compliant model with those of a 2-D rigid Newmark model allows for the quantification of compliance-associated amplifications. A critical parameter effecting plastic displacement amplification in a flexible soil systems is the period of the slide mass. Given the slide mass thickness, mass ratio, and average shear wave velocity, the resonance period, T, of the slide mass can be estimated for an infinite slope or for embankments using the equations of Ambraseys (1960) from his seminal paper on the dynamic response.

For an infinite slope:

$$T = 2\pi(H/V_s) \cdot (m_r)^{0.5}, \tag{16}$$

and for a truncated wedge shaped embankment:

$$T = 4\pi(H/V_s) \cdot (1/a_n) \tag{17}$$

where a_n is tabulated dimensionless coefficient that is a function of the wedge geometry (Ambraseys, 1960).

The Plastic Displacement Spectra (PDRS) describes the maximum plastic displacement of a single degree of freedom system as a function of the natural resonance period and damping. A normalized plot of PDRS is the maximum 2-D plastic displacement of the compliant system divided by the displacement computed for a rigid 2-D system of identical yield acceleration, geometry, and slope. PDRS is similar to the 'slope spectra' concept of Kramer and Smith (1997), and is here computed for maximum slide displacements under multidirectional motions. When the normalized PDRS displacement exceeds 1.0, compliance

effects are amplifying displacements. When they fall below 1.0, compliance effects deamplify displacements.

Two PDRS plots are presented in Fig. 6 for a gentle 4° slope excited by the Newhall motion from the 1994 Northridge Earthquake. The computations are made using uniform 5% and 10% levels of damping within the sliding mass. These plots show the maximum displacement for the 2-D compliant solution with soil mass resonance periods ranging from 0.2-to-2.5 s, normalized by the displacement result for the 2-D rigid Newmark-solution. To make this plot, the PDRS is computed for a suite of single degree of freedom 2-D oscillators and normalized by the rigid 2-D maximum displacements. In this example, when the natural resonance of the compliant slide mass is excited by the motion of the earthquake record (for example, at a period of 0.8 s), the compliant displacements are amplified over those computed by traditional rigid-block Newmark analyses by approximately 25%. At other resonance periods for the sliding mass the resultant deformations can approximate the rigid body solution or be relatively deamplified. The frequency content of a design earthquake motions input to the base of a compliant slope can be estimated through computational site response analysis or by simplified procedures like that of Rathje et al. (1998).

7. Conclusions

This paper explores the combined effects of multidirectional earthquake motions and soil compliance of gently sloping ground of the coastal plain and offshore shelf and slope on seismic displacements. In these environments, strike-directed earthquake motions contribute to dip-directed displacements due to the anisotropic gravitational shear stress of the sloping ground. On level- and gently sloping-ground, including the strike component of motion results in a larger and more accurate shear stress vector than is computed using only the dip-direction of motion. Compliant stresses within the sliding mass influence the applied shear stress on the sliding plane. These compliant stresses can amplify or de-amplify predicted displacements.

This study found that the predicted seismic displacement on gently sloping ground can best be estimated using a multi-parameter model that includes yield acceleration and the peak velocity of the input ground motion. Here, yield acceleration, is presented for soft soils in terms of the Normalized Soil Parameter framework of Ladd and Foott (1974). Compliance effects can be characterized by comparing the compliant block 2-D displacements with those of rigid 2-D block motions under the same earthquake loads, yield acceleration, and slope conditions. Plastic Displacement Response Spectra (PDRS) plots the ratio of the compliant- and rigid-2D displacements against the natural period of resonance of the sliding block. PDRS maps the frequencies where amplification or deamplification of plastic displacements is predicted.
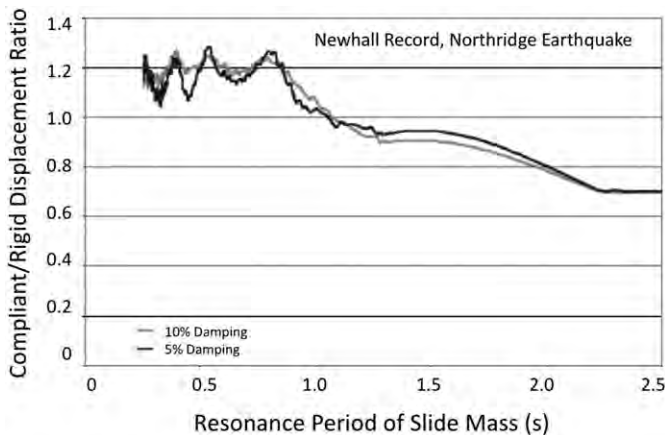
Fig. 6. Plastic Displacement Response Spectra (PDRS) for a range of compliant slide mass periods (abscissa) subjected to the Newhall motion, Northridge 1994 earthquake. The ordinate-axis is the ratio of the displacement for the compliant 2-D model normalized by the corresponding rigid 2-D Newmark model.

References

Ambraseys, N.N., 1960. On the shear response of a two-dimensional truncated wedge subjected to an arbitrary disturbance. Bull. Seismol. Soc. Am. 50 (1), 45–56.
Ambraseys, N.N., Sarma, A.K., 1967. The response of earth dams to strong earthquake. Geotech. Lond. Engl. 17, 181–213.
Arias, A., 1970. A Measure of Earthquake Intensity, Proc. Conf. Seismic Design Nuclear Power Plants. Massachusetts Institute of Technology, pp. 438–483.
Augello, A.J., Bray, J.D., Leonards, G.A., Repetto, P.C., Byrne, R.J., 1995. Response of Landfills to Seismic Loading. Proc. Geoenvironment 2000, ASCE, New York, N.Y vol. 2, pp. 1051–1065.

Boore, D.M., Stewart, J.P., Seyhan, E., Atkinson, G.M., 2014. NGAWest-2 equations for predicting PGA, PGV, and 5%-damped PSA for shallow crustal earthquakes. Earthquake Spectra 30, 1057–1085.

Booth, J.S., O'Leary, D.W., Popenoe, P., Danforth, W.W., 1993. U.S. Atlantic continental slope landslides: their distribution, general attributes, and implications. In: Schwab, W.C., Lee, H.J., Twichell, D.C. (Eds.), Submarine Landslides: Selected Studies in the U.S. Exclusive Economic Zone: U.S. Geological Survey Bulletin No. 2002, pp. 14–22.

Bray, J.D., Repetto, 1994. Seismic design considerations for lined solid waste landfills. Geotext. Geomembr. 13, 497–518.

Bray, J., Travasarou, T., 2007. Simplified procedure for estimating earthquake-induced deviatoric slope displacements. J. Geotech. Geoenviron. Eng.:381–392 http://dx.doi.org/10.1061/(ASCE)1090-0241(2007)133:4(381).

Bray, J.D., Repetto, P.C., Augello, A.J., Byrne, R.J., 1993. An overview of seismic design issues for solid waste landfills. Proc., Geosynthetics Res. Inst. Conf. No. 7. Drexel Univ., Philadelphia, PA.

Bray, J.D., Augello, A.J., Leonards, G.A., Repetto, P.C., Byrne, R.J., 1995. Seismic stability procedures for solid-waste landfills. J. Geotech. Eng. ASCE 121 (2), 139–151.

Chopra, A.K., 2001. Dynamics of Structures. second ed. Prentice-Hall, New Jersey.

Gazetas, G., Uddin, N., 1994. Permanent deformation on preexisting sliding surfaces in dams. J. Geotech. Engrg. ASCE 120 (11), 2041–2061.

Goodman, R.E., Seed, H.B., 1966. Earthquake displacements in sand embankments. J. Soil Mech. Found. Div. SM2, 125–146.

Jibson, R.W., 2007, Regression models for estimating coseismic landslide displacement: Eng. Geol., v. 91, p. 209-218.

Jibson, R.W., Rathje, E.M., Jibson, M.W., Lee, Y.W., 2013. SLAMMER—Seismic LAndslide Movement Modeled using Earthquake Records: U.S. Geological Survey Techniques and Methods 12B1.

Kayen, R.E., Mitchell, J.K., 1997. Assessment of liquefaction potential during earthquakes by Arias intensity. J. Geotech. Geoenviron. Eng. Am. Soc. Civ. Eng. 123 (12), 1162–1175.

Kramer, S.L., Smith, M.W., 1997. Modified Newmark model for seismic displacements of compliant slopes. J. Geotech. Geoenviron. 635–643.

Ladd, C., Foott, R., 1974. NSP Framework for Spol Properties, ASCE FIXME.

Lawson, A.C., 1908. The California Earthquake of April 18, 1906-Report to the State Earthquake Investigation Committee. Carnegie Institute, Washington, D.C. (Pub. 87, chairman).

Lee, H.J., Edwards, B.D., 1986. Regional method to assess offshore slope stability. J. Geotech. Eng. Am. Soc. Civ. Eng. 112, 489–509.

Lee, H.J., Schwab, W.C., Booth, J.S., 1993. Submarine landslides: an introduction. In: Schwab, W.C., Lee, H.J., Twichell, D.C. (Eds.), Submarine landslides: selected studies in the U.S. exclusive economic zone: U.S. Geological Survey Bulletin 2002 1–13.

Lin, J.-S., Whitman, R.V., 1983. Decoupling approximation to the evaluation of earthquake-induced plastic-slip in earth dams. Earthq. Eng. Struct. Dyn. 11 (5), 667–678.

Loukidis, D., Lee, S.-H., Yi, Q., Bourdeau, P.L., 2001. Analytical Study of the Nikawa Landslide. International Conferences on Recent Advances in Geotechnical Earthquake Engineering and Soil Dynamics. Paper 20.

Makdisi, F.I., Seed, H.B., 1978. Simplified procedure for estimating dam and embankment earthquake-induced deformations. J. Geotech. Eng. Div. ASCE 104 (7), 849–867.

Newmark, N.M., 1959. A method of computation for structural dynamics, EM3. J .Eng. Mech. Div. 67–94.

Newmark, N.M., 1965. Effects of earthquakes on dams and embankments. Geotech. Lond. Engl. 15 (2), 139–160.

O'Rourke, T.D., 1998. An Overview of Geotechnical and Lifeline Earthquake Engineering. In: Dakoulas, P., Yegian, M. (Eds.), Geotechnical Special Publication No. 75, Proc. Of Geotechnical Earthquake Engineering and Soil Dynamics Conference Held in Seattle, Washington, Aug. 1998 vol. 2. ASCE, Reston, Virginia, pp. 1392–1426.

Rathje, E.M., Bray, J.D., 2000. Nonlinear coupled seismic sliding analysis of earth structures. J. Geotech. Geoenviron. 126, 1002–1014.

Rathje, E., Abrahamson, N.A., Bray, J.D., 1998. Simplified frequency content estimates of earthquake ground motions. J. Geotech. Geoenviron.

Seed, H.B., 1979. Considerations in the earthquake-resistant design of earth and rockfill dams, 19th Rankine Lecture of the British Geotechnical Society. Geotechnique XXXIX (3), 215–263 (September 1979).

Seed, H.B., Martin, G.R., 1966. The seismic coefficient in earth dam design, GT3. J. Geotech. Eng. Div. 25–58.

Seed, H.B., Lee, K.L., Idriss, I.M., Makdisi, F., 1973. Analysis of the slides in the San Fernando Dams during the earthquake of Feb. 9, 1971. Report EERC 73-2, Earthquake Engineering Research Center, University of California, Berkeley.

Trifunac, M.D., Todorovska, M.I., 1997. Northridge, California, earthquake of 1994: density of pipe breaks and surface strains. Soil Dyn. Earthq. Eng. 16, 193–202.

Wilson, R.C., Keefer, D.K., 1985. Predicting Areal Limits of Earthquake-induced Landsliding. In: Ziony, J.I., (Ed.), Evaluating the Earthquake Hazards in the Los Angeles Region 1360. Geological Survey Professional Paper, U.S.

Wood, D.M., 1991. Soil Behaviour and Critical State Soil Mechanics. Cambridge University Press 0521332494 (488 pp.).

Zhang, J., Andrus, R.D., Juang, C.H., 2005. Normalized shear modulus and material damping ratio relationships. J. Geotech. Geoenviron. Eng. ASCE 131 (4):453–464. http://dx.doi.org/10.1061/(ASCE)1090-0241(2005)131:4(453).